IIETA International Information and Engineering Technology Association
Advancing the World of Information and Engineering

Revue des Composites et des Matériaux Avancés-Journal of Composite and Advanced Materials
Vol. 32, No. 6, December, 2022, pp. 285-293
Journal homepage: http://iieta.org/journals/rcma

Grain Boundary and Microstructural Characterization of Heat-Treated As-Rolled 2205 Duplex Stainless Steel

Mamookho E. Makhatha*, Akinsanya D. Baruwa, Elvis Gonya

Department of Metallurgy, University of Johannesburg, Johannesburg 2094, South Africa

Corresponding Author Email: emakhatha@uj.ac.za

https://doi.org/10.18280/rcma.320604

Received: 2 August 2022
Accepted: 5 October 2022

Keywords:
austenite, duplex stainless steel, equiaxed, ferrite, grain boundary, microstructure, Widmanstätten

ABSTRACT

The detrimental precipitation at the 2205 duplex stainless steel (DSS) grain boundaries has characterized the material to have poor workability after being hot-rolled. However, the detrimental precipitation in the microstructure is largely influenced by the cooling rate or method. There is an insufficient investigation of this steel's grade interfaces and grain boundaries to rationale its poor workability. This study investigates the influence of heat treatment of hot-rolled 2205 DSS to eliminate the precipitation at the grain boundaries and a detailed microstructural study. The procedure was carried out by heat-treating the as-rolled 2205 DSS to achieve the equiaxed and Widmanstätten austenite morphologies. The characterization was conducted using an optical microscope, electron backscatter diffraction and X-ray diffraction. It was found that the Widmanstätten morphology carried a high fraction of austenite-ferrite interfaces and high grain boundary responsible for the steel cracking during hot rolling. The SEM analysis observed an incoherent interface in Widmanstätten morphology, while the equiaxed demonstrated a coherent interface. XRD detailed new phases such as martensite and cementite in Widmanstätten and equiaxed morphologies, respectively. The Widmanstätten will quickly be susceptible to crack initiation under the application.

1. INTRODUCTION

Metal such as duplex stainless steel 2205 possesses an equivalent amount of ferrite and austenitic phases. The phases formed the basis for improved strength, including ductility [1-3]. Previous research has demonstrated that 2205 DSS has exceptional intrinsic and functional attributes. The outstanding characteristics of 2205 duplex stainless steel have attracted and continue to attract a vast number of users for different applications such as antimicrobials [4], industrial-marine environment [5], and hemocompatibility [6], to mention a few. Its extensive use results from its alloying elements, such as molybdenum and chromium, which are resistant to corrosion and oxidation processes [7]. Due to these excellent properties, the DSS 2205 is broadly applied in the petrochemical, oil and gas, chemical, and desalination sectors, including maritime environments [7-9].

However, the intrinsic mechanical properties and functionality could improve or depreciate after heat treatment or hot deformation [10, 11]. The improvement or depreciation is caused by the change in the bulk materials' microstructure, morphology and phase orientations. Although, the hot-rolling, heat treatment or hot-deformation process is known to cause changes in the characteristics of materials. For example, when magnesium ZEK100 alloy was subjected to hot rolling at temperatures from 350°C to 450°C, there was grain refinement as a result of thermo-mechanical processing, and it improved both the ultimate tensile strength and yield strength [12]. Elongated grains of the primary Alpha (α) phase at 790°C and Beta (β) at 870°C rolling temperatures were seen in high-strength beta titanium alloy [13]. β-stabilised ′Y-TiAl based alloy hot-rolled at temperatures; 1200°C, 1250°C and 1350°C showed that the grains became coarsened and elongated along the rolling direction [14]. It is also worth knowing that 10 Mn steel warm-rolled from 250°C to 600°C also caused changes in the microstructure and eventually caused improvement in the mechanical properties [15]. Heat treatment of laser melted 316L steel caused a lower fatigue life of the material [16]. A reduced hardening rate is observed at elevated temperatures for both A6061 and A6063 aluminum alloys [17]. These changes in properties are based on the interactions of the grains in the microstructures. The precipitation of °detrimental phases in the microstructure has been reported to either impact or have no effect on the yielding properties [18-20].

The interior structure of crystals is said to contain a network of interfaces known as grain boundaries. Its presence and design have an effect on a material's mechanical characteristics and overall functionality [21]. The three forms of boundaries associated with materials are low angle grain boundaries (LAGB), high angle grain boundaries (HAGB), and special high angle grain boundaries (SHAGB). Tilt and twist angle grain boundaries are divisions of LAGB. HAGB are created when the dislocation cores of low-angle tilt boundaries cross at an angle greater than 15° [22]. These limits have a haphazard, or more accurately, uneven structure [23]. Boundaries with a high orientation and a high density of coincidence locations relationship are referred to as SAGB [24]. The rate at which grain boundaries move tells us what propels them in that direction [18]. This movement leads to the microstructure of polycrystalline materials. Even though the

physics of grain boundary migration is unclear, it thus depends on atoms passing through grain boundaries to gain energy. At low-angle grain boundaries (LAGB), migration is caused by cross- and slide-dislocations [25]. However, dynamic recovery happens due to grain boundary displacement because dynamic recrystallization does not proceed [26]. In low stacking fault metals, grain boundary migration results in dynamic recrystallization due to an increase in dislocation density, which restricts dynamic recovery [26]. Coherent, semi-coherent, and incoherent interfaces are the interfaces that can exist in metal. These groups of interfaces are visible in the equiaxed and Widmanstätten austenite morphologies of 2205 duplex stainless steel: the austenite-ferrite (A/F), ferrite-ferrite (F/F), and austenite-austenite (A/A) interfaces. Heterophase interfaces called A/F interfaces mimic metal interfaces, while solid-solid interfaces are associated with the A/A or F/F interfaces [27]. Furthermore, the resulting grain of A/F exhibits a Kurdjumov-Sachs (K-S) orientation relationship when phase transition occurs. This is indicated by a rotation of the angle of the crystallographic axis [28]. The orientation connection boosts its ductility by altering the deformation behaviour and hot workability of 2205 DSS [29].

There is still a dearth of investigation on the effects of heat treatment on the abolition of precipitation of hazardous phases on the DSS 2205 equiaxed and Widmanstätten austenite morphologies. Previous studies conducted did not critically unravel what happens at the interfaces and subgrain levels. They rather focused on the macroscopic behaviour of heat-treated hot rolled 2205 DSS in applications such as corrosion resistance [30, 31], strength, wear resistance [32] and crack resistance if inclusions are avoided [33]. Some researchers investigated grains evolution and interface relationship but did not examine changes in phase after heat treatment [34, 35]. Therefore, the 2205 DSS grains will be characterized to determine the boundaries, interfaces and phases that may exist after heat treatment which could further influence its properties.

Here, the microstructure of the heat-treated as-rolled 2205 DSS is characterized using three different image analyses, including electron backscatter diffraction (EBSD) technology which establishes a stereological-based analysis. It does measure all parameters and statistics associated with microstructure and micrographs, including mono- and poly-crystalline materials [36]. The characterization would be supplemented by x-ray diffraction. To properly investigate the characteristics (grains, boundaries, interfaces and the microstructure) of 2205 DSS, at least two morphologies are required for adequate comparison and relativity. These methods are used to demonstrate that the heat treatment eliminates detrimental phases and establishes the formation of both intragranular and intergranular grains. Also, additional phases, such as cementite and martensites, depend on the cooling after heat treatment.

The study will assist engineers and scientists in understanding the behaviour of this material when subjected to heat treatment and enable the development of an efficient microstructure and properties for a particular application.

2. MATERIALS AND METHOD

2.1 Material

Metal Centre in Gauteng, South Africa, supplied the 2205 duplex stainless steel sample. The as-received was in slab and then formed into a 10mm diameter cylindrical bar.

2.2 Heat treatment

The as-rolled material was solution heat-treated to form a DSS microstructure with equiaxed and Widmanstätten austenite morphologies. The treatment was carried out in a controlled environment using a tube furnace to avoid oxidation during heating. The material was heated at the rate of 10℃/s from 25℃ to a region of single-phase delta ferritic with a temperature of 1340℃. After reaching 1340℃, there were 40 minutes of holding to ensure delta ferritic microstructure was attained. The specimens were then cooled in the furnace to 970℃ at the rate of 0.002℃/s. The cooling was achieved in 48 hours, and then the samples were subjected to rapid cooling in water to achieve equiaxed morphology. The goal of rapid cooling from 970℃ was to avoid the creation of harmful phases within 800 - 400℃. Figure 1 depicts a pictorial representation of the process. In the case of Widmanstätten morphology, the sample was rapidly cooled after solution treatment at 1340℃.

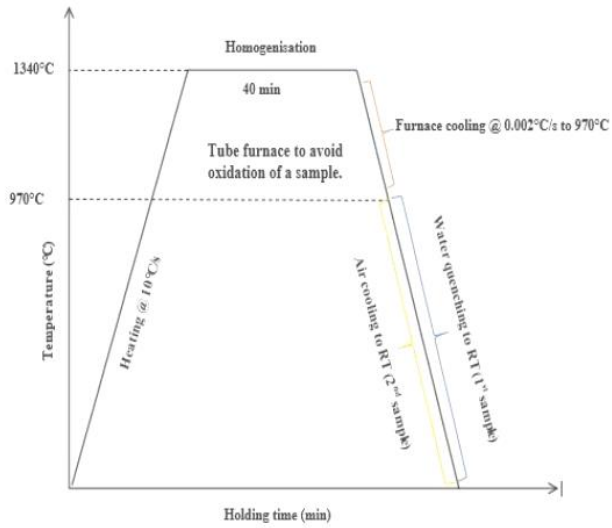

Figure 1. Solution heat treatments of 2205 DSS to obtain equiaxed and Widmanstätten austenite morphologies

2.3 Characterizations

For accurate characterization, the samples were prepared according to standards ASTM E3-01, ASTM E7-03, and ASTM E407-99. A ZEISS VisionSE64 optical microscope was utilized for phase identification. For the microstructure and grain boundary analysis, Merlin VP Compact scanning electron microscope equipped with HKL EBSD technology operated at 20kV, 7nA electron beam size and electron beam detector at 0.00° tilt was used. The comprehensive orientation maps' dimensions were determined at 1.05mm in width and 1.4mm in height to investigate the substructure properties. The process had a dwell time of 19 µs. X-ray diffraction investigation was carried out on the heat-treated 2205 DSS in order to identify phase compounds. Using Rigaku Ultima IV, the patterns were acquired by scanning from 5° to 90° equal 2-theta angle at 0.5°/min with an XRD diffraction. The x-ray source's voltage, current, and wavelength were set to 40kV, 30mA, and 1.54, respectively. The PDXL software was used to analyze the data.

3. RESULTS AND DISCUSSION

3.1 Microstructure

3.1.1 Scanning electron microscope

For the investigation of the grain distribution, an optical microscope was used at low magnifications, Figure 2. The images were taken at low magnification to ascertain the phases in the microstructure. Figure 2a represents the microstructure of the as-rolled 2205 DSS, while Figure 2b displays the Widmanstätten morphology and Figure 2c as the equiaxed microstructure. Both Figures 2a and 2b are attained after the systemic cooling down process.

The as-rolled 2205 duplex stainless steel grains in Figure 2a appear to be significantly pan-caked in both ferrite and austenite grains. The ferrite grains, which are dark grey, are surrounded by light grey austenite grains are plastically elongated in the direction of rolling. Due to compression during rolling, the austenitic grain showed mixed continuous and discontinuous lamellae structures. The exterior and core of the as-rolled showed to be compact and continuous, while in-between (core) morphology showed to be discontinuous though the grains were elongated. The occurrence of this kind of structure is a result of the existence of low stack energy between the austenite-ferrite when compared with ferrite-ferrite or austenite-austenite grain [37]. The Widmanstätten morphology in Figure 2b shows ferrite and austenite of needle-like structure as well as dendritic in nature as a result of the accelerated cooling after heat treatment. The Widmanstätten austenite nucleates discretely on the austenite allotriomorphs grain boundaries and also grows on the ferrite matrix by a diffusional mechanism with a close Kurdjumov–Sachs orientation relationship [38]. Kurdjumov-Sachs orientation is ideal because the lattice planes between the 100-planar of ferrite and the 111-planar of the austenite correspond. From Figure 2b, it is evident that both the intragranular and intergranular austenite are formed. The austenite grows in this region, and the defect-free phase barrier results in a good transition between the phases [36]. Figure 2c illustrates the ferrite and austenite grains produced when the sample was heated to 1350℃, allowed to homogenize for 40 minutes, and then quickly cooled to 1000℃ to produce an equiaxed structure. After heat treatment, the equiaxed microstructure recovered from elongated structures back to rigid and discrete phases. Therefore, the equiaxed structure underwent recrystallization. The secondary austenite was generated as a result of the hot-rolling process and dissolved into ferrite in both morphologies. This process is enabled by the reduced Kurdjumov-Sachs fractions produced as a result of slow cooling associated with the microstructure. Therefore, it means that after heat-treating hot-rolled 2205 DSS, the secondary austenite-ferrite transition occurred prior to the primary austenite-ferrite transition, thereby making all the secondary austenite transmogrified to ferrite before the completion of heat-treatment.

3.1.2 Scanning electron microscope

The chemical composition was determined by energy-dispersive spectrometry (EDS) attached to the scanning electron microscope (SEM) as a first step toward identifying the phases in equiaxed and Widmanstätten structures [39]. The outcomes of EDS studies of the phases are shown in Figure 3 and detailed in Table 1. According to the EDS investigations, the primary balance phases of ferrite and austenite were correctly detected.

According to previous studies, chromium, nickel, and molybdenum increase steel's ability to resist corrosion, including pitting and crack corrosion [9]. Chromium and molybdenum are ferrite formers, while manganese, nickel, and nitrogen are austenite stabilizers. The EDS study of the microstructure of the hot-rolled 2205 DSS demonstrates the partitioning of elements between the ferrite and the austenite, and it is consistent with the findings of ferrite transforming into austenite. In Table 1, the ferrite formers are distributed into the old ferrite phase according to their chemical compositions of 23.10 and 01.75%, respectively. In contrast, the austenite stabilizers are transformed into coarsened austenite, which is demonstrated by their greater chemical compositions of 05.10 and 01.82% in Table 1.

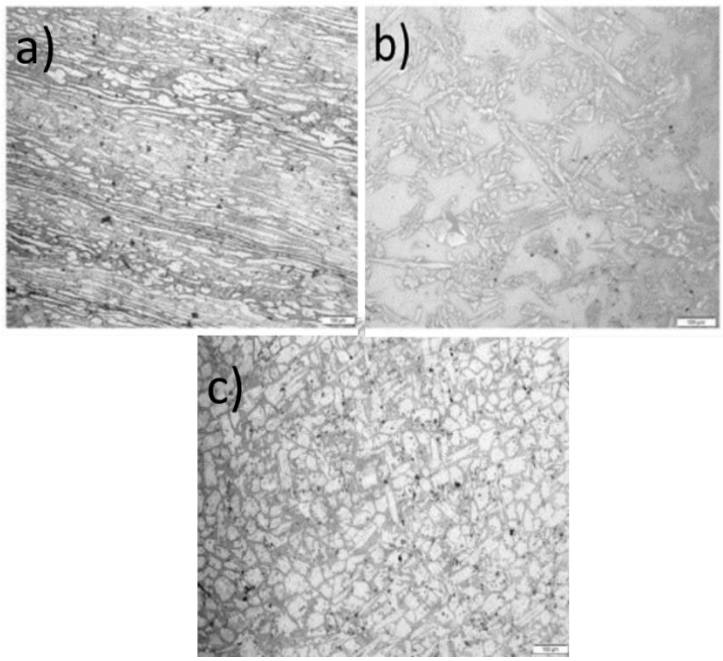

Figure 2. Microstructure of 2205 DSS taken at 100 μm of a) as-rolled, b) Widmanstätten and c) equiaxed

Table 1. Elements of normalized analyzed by SEM/EDS

Element	Equiaxed		Widmanstätten	
	Ferrite (%)	Austenite (%)	Ferrite (%)	Austenite (%)
C	0.00	0.00	03.84	04.28
Si	0.31	0.00	0.32	0.33
Cr	21.15	22.66	23.10	21.21
Mn	01.38	21.63	01.75	01.82
Fe	61.70	02.41	63.32	62.76
Ni	03.82	0.23	0.00	05.10
Mo	0.00	0.00	0.00	02.64

The ferrite formers are partitioned to the old ferrite phase as well, whereas nickel and manganese, the austenite stabilizers, are converted to the coarsened austenite. In Figures 3a and c, iron (Fe) and chromium (Cr) displayed the largest peaks. The situation exists due to the size of the precipitate at the sub-micron scale and interaction with the ferrite matrix. The amounts of chromium and nickel are listed for the ferrite and austenite phases in Table 1. The lack of balance when ferrite changed into austenite may have been primarily caused by the low nickel concentrations, which could contribute to its poor hot workability. As previously indicated, the transition from ferrite to coarsened austenite was caused by the weaker inter-atomic bonds brought about by elevated temperatures. The matching lattice planes between the ferrite and austenite (100 and 111) enable this change. In the ensuing microstructure, the coarse austenite formed more sporadic contact with the A/A, F/F, and A/F interfaces [40].

3.1.3 Electron back-scattered diffraction

EBSD phase mapping was done on a 1.47mm^2 area and presented in Figure 4. The three constituents visible on the phase map are the Fe-BCC, Fe-FCC, and minor percentages of TiC lining around the coarse BCC grain boundaries. Table 2 displays the mapping statistics for the area of interest. A higher percentage of iron FCC, 67.72%, is present and is in accordance with the microstructure. According to the microstructure in 4b, a higher fraction of iron FCC-67.72% is present, while the BCC fraction was discovered to be 28.96%. The high iron FCC fractions suggest that austenite is more prevalent than ferrite. It was established that low stacking fault energy causes the reduction in mobility of dislocations at grain boundaries associated with austenite. Due to the significant proportions of austenite, it is therefore expected that the corresponding grain boundaries are stationary [41]. The locations at which the electron beam of the SEM with EBSD was unable to detect fractions are represented by the zero solution in Table 2.

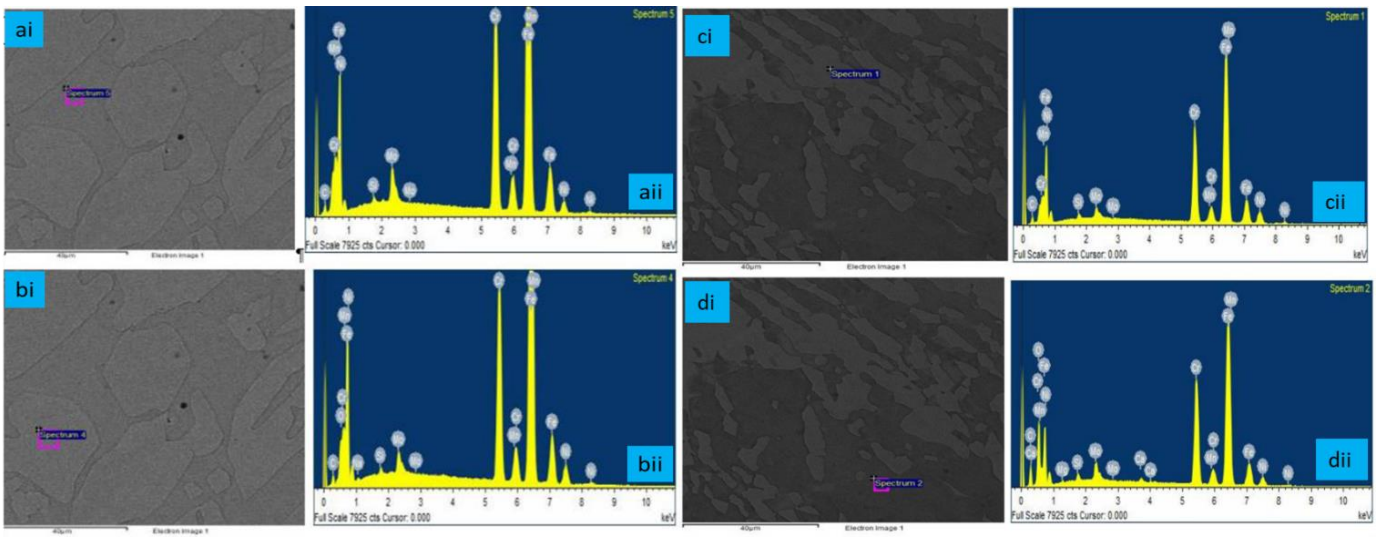

Figure 3. Represents the SEM morphology (i) and the corresponding EDS (ii) analysis of 2205 duplex stainless steel for a) equiaxed ferrite phase, b) equiaxed austenite phase c) Widmanstätten austenite phase, and d) Widmanstätten ferrite phase

Table 2. Full-mapping statistics of the heat-treated 2205 DSS

Microstructure	Phase Type	Phase Fraction (%)	Phase count	Mean MAD	Standard Deviation MAD
Equiaxed	Fe- BCC (old)	28.96	4128	0.77	0.12
	Fe-FCC	67.72	9654	0.80	0.12
	TiC	0.33	47	0.84	0.09
	Zero Solutions	3.00	427		N/A
Widmanstätten	Fe-BCC (old)	60.79	6128	0.64	0.13
	Fe-FCC	24.24	2443	0.72	0.11
	TiC	0.04	4	1.36	0.78
	Zero Solutions	14.93	1505		N/A

∗MAD= mean angular deviation

An inverse pole figure is a two-dimensional graphical depiction of the orientation of a selected plane that is relatively normal to the sample reference frame. The mapping obtained from the analysis results in the microstructural evolution in the X, Y, and Z directions, as shown in Figure 5 (a, b, and c) for as-rolled, equiaxed and Widmanstätten. The as-rolled grains, Figure 5a, demonstrated a deficient stage orientation of A/F grain distribution along 111 and 110 planar with respect to XYZ coordinates. It is a testament to the fact that the interface is incoherent due to the random orientation of the nucleus

matrix. The orientation is induced by the deformation the material suffered after hot-rolling. In Figure 5b, the iron BCC dominates the matrix, and the iron FCC makes up the coarsened grains. With reference to Figure 5, the IPF orientation triangle is utilized to depict the direction in which these grains orient. Because the green grains in this example transpose to the blue grains, the grains are orientated in the [111] direction. The purple grains also transpose to the blue grains in Figure 5b; the grains are oriented towards the [100] direction.

Furthermore, the grains also aligned in the [110] direction. In a polycrystalline ferrite matrix, plate-like monocrystal austenites are distributed almost randomly in space. They are orientated in accordance with the Kurdjumov-Sachs relationship when the interface possesses semi-coherent interphase boundaries, according to Zhang [34]. The K-S relationships between (011) Ferrite/(111) austenite planar and (111) Ferrite/(110) austenite planar can also be used to establish the Nishiyama-Wassermann (N-W) relationship by rotating (011) Ferrite by 5.26° [42]. Due to the semi-coherent interfaces that Widmanstätten have, these semi-coherent interfaces go from semi-coherent to incoherent following the rolling process.

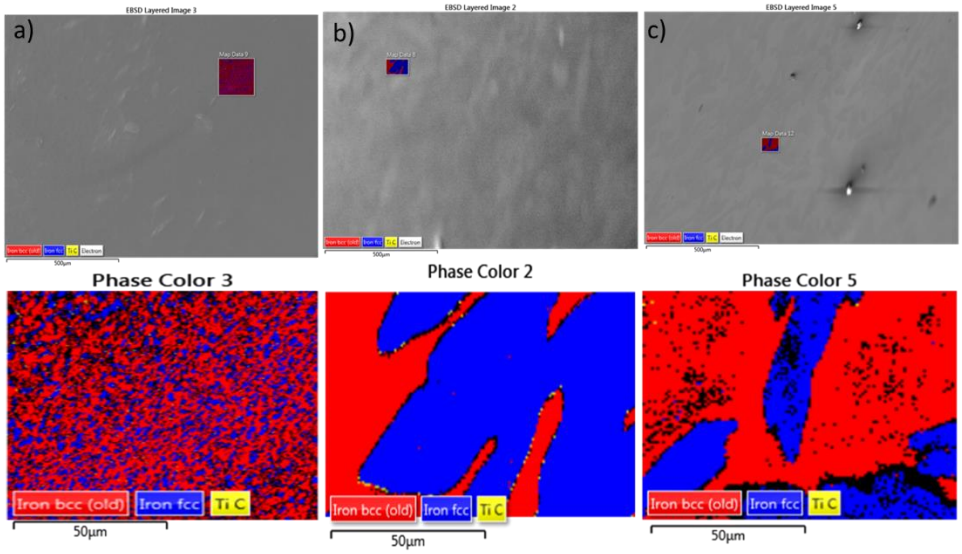

Figure 4. The EBSD mapping of the yielded microstructure of a) as-rolled, b) equiaxed, and c) Widmanstätten

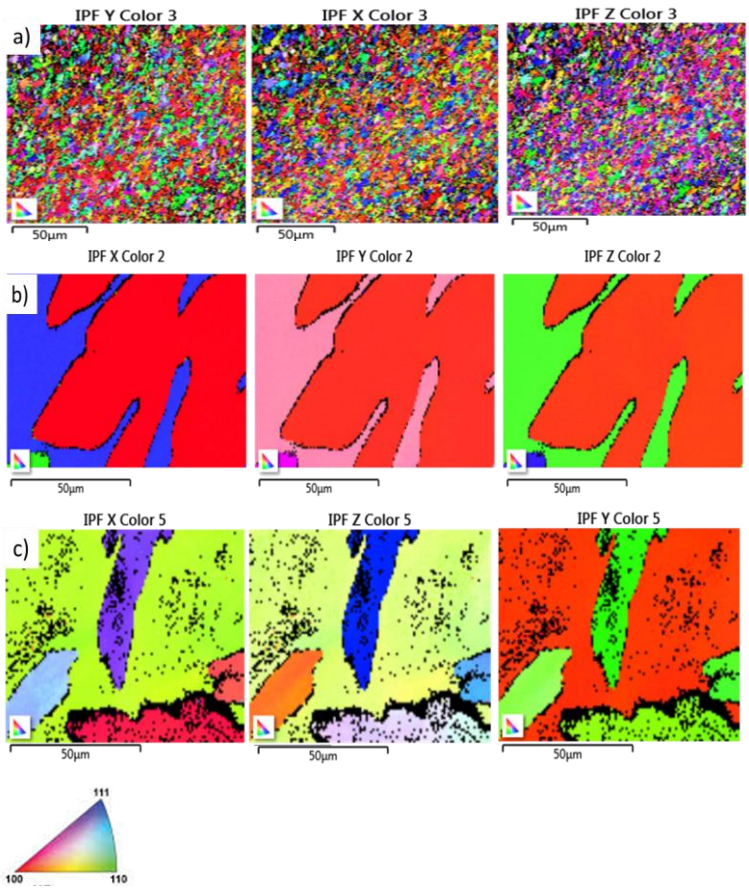

Figure 5. Inverse pole figures in the x, y, and z directions of the a) as rolled, b) the equiaxed, and c) the Widmanstätten

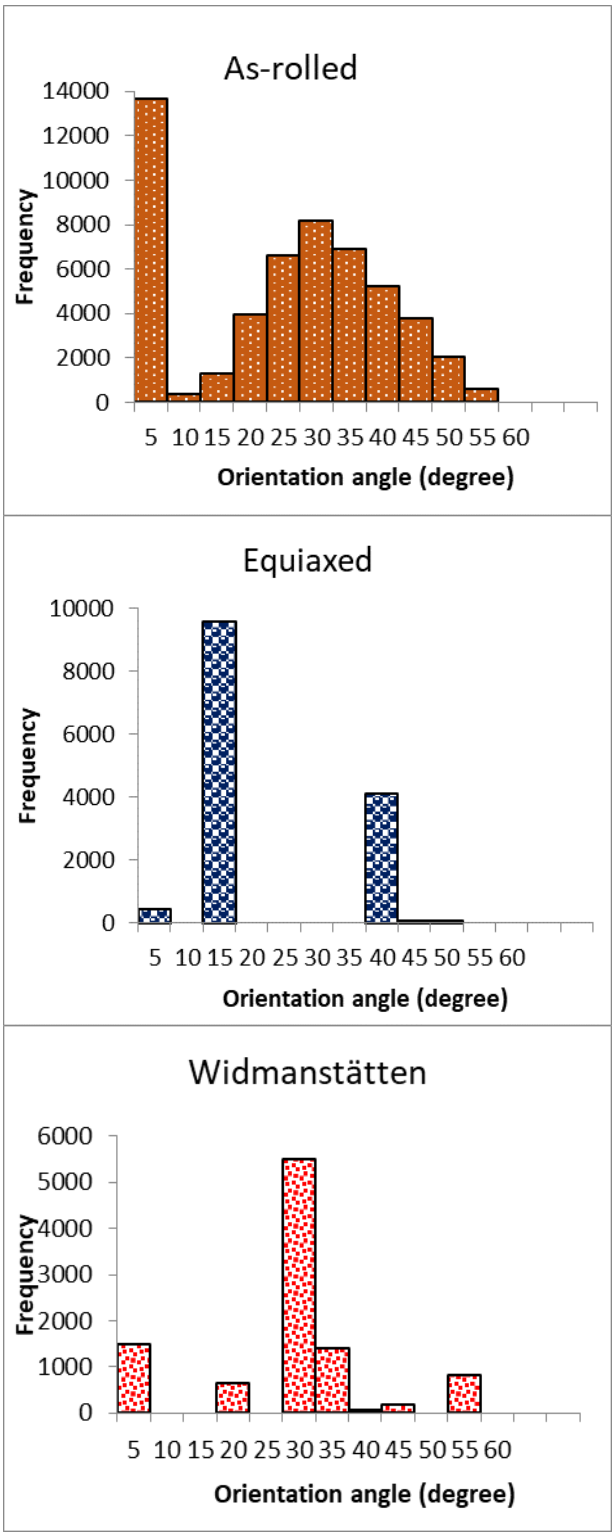

Figure 6. Grain orientation of the as-rolled, equiaxed and Widmanstätten after heat-treatment of the as-rolled

Figure 6 shows a frequency distribution plotted against the orientation angle for the as-rolled, equiaxed austenite and Widmanstätten morphologies. The as-rolled showed mixed and alternate low and high grain boundaries having orientation angles from 0° to 55°, with orientation within 5° being predominant. This orientation within 5° results from grain breakage emanating from the rolling process. According to the literature, high angle grain boundaries are visible when $\theta > 15°$ and low angle grain boundaries are visible when $\theta < 15°$ [43]. The equiaxed indicates that the LAGB predominate in the microstructure since the largest peak is seen when the angle is less than 15°. Dislocations are placed sporadically along the grain borders. Additionally, these grain boundaries are located in regions where crystals fit together perfectly. As a result, the low-angle grain boundaries have a cohesive interface. The interfaces that result from the exact alignment of two crystals at the interface planes are known as coherent interfaces [44]. These interfaces will have low interfacial energy, which is insufficient to support dislocation climbing, resulting in static grain boundaries.

However, the Widmanstätten structure displayed almost purely high grain angles as the angle is greater than 15°. The Widmanstätten histogram is dispersed to the right having predominant grains within 25° – 30°. With a high percentage of high-angle grain boundaries, Widmanstätten austenite is likely to crack since these borders will have high interfacial energy, which will facilitate the climbing and cross-slipping of the grain boundaries. It will be least workable at 2205 DSS during hot workability. It also carries an incoherent nature that does not prevent grain boundaries from sliding. High grain boundaries also pose to have excessive hardness and internal strength at the expense of ductility and toughness, thereby subjecting the grain to the point of crack initiation [44]. It is more likely that the steel will crack because of the incoherent interfaces' K-S orientation connection that prevents the sliding of grain boundaries. The lack of hot workability of the steel is further explained by the incoherent nature and K-S orientation connection of austenite-ferrite (A/F) interfaces, which suggests that a higher percentage of A/F interfaces have these characteristics.

3.2 X-ray diffraction

Figure 7 shows the as-received 2205 DSS, normalized (equiaxed), and quenched (Widmanstätten) sample's diffraction pattern. The purpose of the XRD was to identify the phases present in each sample after the heat treatment.

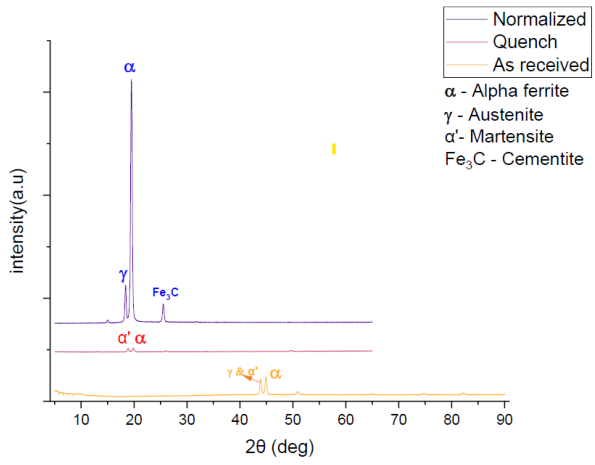

Figure 7. The phase evolution and identification of as-rolled 2205 DSS and heat-treated 2205 DSS using XRD

In the as-rolled sample, three phases were identified: alpha ferrite, gamma austenite, and martensite. This contradicts the results obtained from the optical micrograph. Falodun [31] asserts that during the hot rolling of 2205 DSS, strain-deformation causes the austenite phase to change into the martensite phase. Based on Bain's theory, heat treatment can

turn martensite back into the austenite phase because the 2205 DSS only needs the ferrite and austenite phases. Hence, applying heat converts the martensite phase to the austenite phase [45]. In order to determine whether any intermetallic phases in the Widmanstätten structure might impair the functionality or use of the 2205 DSS, an XRD was conducted on the heat-treated sample. Two phases were found; martensite is profound at 76.10%, and the volume fraction of the austenite is around 23.89%. During rapid cooling, the presence of C and N led to the precipitation of the martensite phase, which tends to harden the 2205 DSS. Therefore, rapid cooling causes a rise in martensite formation [46]. The high-volume martensite component will increase the hardness of 2205 DSS, making the material brittle and prone to cracking when subjected to stress.

Martensite is formed when austenite cools quickly and traps carbon atoms that can't exit the crystal structure. The parent phase- austenite, becomes mechanically unstable when it reaches the martensite temperature [47]. Generally, martensite is formed during annealing at temperatures lower than 400°C. The austenite volume proportion in the equiaxed sample is large since the amount of ferrite stabilizer components in the chemical composition has decreased (Ni and Cr). The three phases were detected with the equiaxed structure: ferrite, austenite, and a small quantity of cementite. The volume fraction of the ferrite phase was found to be 58.7%, the austenite phase, 40.3%, and the cementite phase, 0.92%. The presence of cementite could be a result of cooling to room temperature. The carbon that did not retain in the solid solution during the ferrite phase formed cementite, preventing the carbon from evaporating as free carbon [48]. The modest volume proportion of cementite will only slightly increase the hardness of 2205 duplex stainless steel.

From the observation, both samples have no detrimental phases detected by the XRD, indicating that neither structure creates detrimental phases such as the sigma phase, chi phase, or alpha prime. Furthermore, there were no intermetallic phases observed. The equiaxed sample will not quickly fail due to its greater ductility potential during the application, while the Widmanstätten sample, which has a higher volume fraction of martensite, could result in brittle failure during application.

4. CONCLUSIONS

2205 DSS is associated with poor hot workability. Hence, the effect of the cooling method on the microstructural evolution is successfully characterized. The goal also characterizes the grain boundaries that exist in the microstructures which define its functionality. After cooling, the equiaxed and Widmanstätten austenite morphologies are yielded. The rapid cooling associated with water quenching completely transformed the austenite phase into martensite. This resulted in a volume fraction of 76.10%, which can increase the hardness of the 2205 DSS. In contrast, the normalized quenching process only partially transformed the austenite phase into cementite; and culminated in a volume fraction of 0.92%, which could reduce the hardness of the 2205 DSS. The precipitation of the detrimental phases was not observed in both morphologies. Furthermore, from the microstructural observations, adequate and accurate heat treatment eliminates austenite protrusions usually associated with low-angle sub-boundaries. The cooling method demonstrated its effect on the yielded Widmanstätten morphology as there are large numbers of partially transformed austenite in the matrix observed due to the dissolution of the austenite. The EBSD data indicated that both morphologies oriented more toward 111- planar to establish its austenite intervariant boundaries plane distribution. The XRD analysis results showed no initiation of the detrimental phases, such as chi, sigma, and alpha prime, in both microstructures. This means that the 2205 duplex stainless steel will not be susceptible to cracking because of detrimental phases. Due to the different cooling methods, phases such as martensite and cementite are present in Widmanstätten and equiaxed morphologies, respectively. The formation of martensite in the Widmanstätten morphology could result from low carbon content in the chemical composition of 2205 DSS. The equiaxed structure will enhance sliding and minimize cracks associated with hot rolled 2205 DSS while Widmanstätten obeys an ideal K-S relationship. It is clear that heat treatment also causes the recrystallization of grains in structures. Heat treatment of hot-rolled 2205 DSS will eliminate poor hot working conditions related to hot-rolled 2205 DSS.

Therefore, the equiaxed structure will function better in hot-working conditions compared to the morphology associated with Widmanstätten.

ACKNOWLEDGMENT

The authors want to thank the University of Johannesburg and Transnet South Africa for this project's equipment and financial support.

REFERENCES

[1] Kahar, D.S.D. (2017). Duplex stainless steels-an overview. International Journal of Engineering Research and Applications, 7(4): 27-36. https://doi.org/10.9790/9622-0704042736

[2] Cheng, X., Wang, Y., Li, X., Dong, C. (2018). Interaction between austein-ferrite phases on passive performance of 2205 duplex stainless steel. Journal of Materials Science and Technology, 34(11): 2140-2148. https://doi.org/10.1016/j.jmst.2018.02.020

[3] Makhdoom, M.A., Ahmad, A., Kamran, M., Abid, K., Haider, W. (2017). Microstructural and electrochemical behavior of 2205 duplex stainless steel weldments. Surfaces and Interfaces, 9: 189-195. https://doi.org/10.1016/j.surfin.2017.09.007

[4] Zhao, Y., Zhou, E., Xu, D., Yang, Y., Zhao, Y., Zhang, T., Gu, T., Yang, K., Wang, F. (2018). Laboratory investigation of microbiologically influenced corrosion of 2205 duplex stainless steel by marine pseudomonas aeruginosa biofilm using electrochemical noise. Corrosion Science, 143: 281-291. https://doi.org/10.1016/j.corsci.2018.08.018

[5] Zhang, T., Zhao, Y.G., Dong, B.J., Li, X.G. (2020). Corrosion behaviour of 2205 DSS in the artificial industrial-marine environment. Corrosion Engineering Science and Technology, 56(1): 22-34. https://doi.org/10.1080/1478422X.2020.1793468

[6] Mahajan, A., Sidhu, S.S., Devgan, S. (2020). Examination of hemocompatibility and corrosion resistance of electrical discharge-treated duplex stainless

steel (DSS-2205) for biomedical applications. Applied Physics A: Materials Science and Processing, 126(9): 737. https://doi.org/10.1007/s00339-020-03940-5

[7] Park, J.S., Cho, D.M., Hong, S.G., Kim, S.J. (2021). Effects of reducing atmospheres of bright annealing on the surface and corrosion characteristics of super duplex stainless steel tubes. Surface and Coatings Technology, 423: 127621 https://doi.org/10.1016/j.surfcoat.2021.127621

[8] Verma, J., Taiwade, R.V. (2017). Effect of welding processes and conditions on the microstructure, mechanical properties and corrosion resistance of duplex stainless steel weldments—a review. Journal of Manufacturing Processes, 25: 134-152 https://doi.org/10.1016/j.jmapro.2016.11.003

[9] Vinoth Jebaraj, A., Ajaykumar, L., Deepak, C.R., Aditya, K.V.V. (2017). Weldability, machinability and surfacing of commercial duplex stainless steel AISI2205 for marine applications – a recent review. Journal of Advanced Research, 8(3): 183-199. https://doi.org/10.1016/j.jare.2017.01.002

[10] Tavares, T.B., Rodrigues, D.G., Santos, D.B. (2020). Effect of warm rolling and annealing on microstructure, texture, and mechanical properties of a 2205 Duplex Stainless Steel. Steel Research International, 91(4): 1-11. https://doi.org/10.1002/srin.201900543

[11] Yan, M., Sun, J.N., Huang, H.G., Chen, L., Dong, K., Chen, Z.Y. (2018). Effect of hot rolling and cooling process on microstructure and properties of 2205/Q235 clad plate. Journal of Iron and Steel Research International, 25(11): 1113-1122. https://doi.org/10.1007/s42243-018-0172-6

[12] Javaid, A., Czerwinski, F. (2019). Effect of hot rolling on microstructure and properties of the ZEK100 alloy. Journal of Magnesium and Alloys, 7(1): 27-37. https://doi.org/10.1016/j.jma.2019.02.001

[13] Du, Z.X., Xiao, S.L., Shen, Y.P., Liu, J.S., Liu, J., Xu, L.J., Kong, F.T., Chen, Y.Y. (2015). Effect of hot rolling and heat treatment on microstructure and tensile properties of high strength beta titanium alloy sheets. Materials Science and Engineering A, 631: 67-74 https://doi.org/10.1016/j.msea.2015.02.030

[14] Erdely, P., Staron, P., Maawad, E., Schell, N., Klose, J., Mayer, S., Clemens, H. (2017). Effect of hot rolling and primary annealing on the microstructure and texture of a β-stabilised γ-TiAl based alloy. Acta Materialia, 126: 145-153 https://doi.org/10.1016/j.actamat.2016.12.056

[15] Hu, B., Tu, X., Luo, H., Mao, X. (2020). Effect of warm rolling process on microstructures and tensile properties of 10 Mn steel. Journal of Materials Science and Technology, 47: 131-141. https://doi.org/10.1016/j.jmst.2019.12.026

[16] Kluczyński, J., Śnieżek, L., Grzelak, K., Torzewski, J., Szachogłuchowicz, I., Oziębło, A., Perkowski, K., Wachowski, M., Małek, M. (2020). The influence of heat treatment on low cycle fatigue properties of selectively laser melted 316l steel. Materials, 13(24): 5737. https://doi.org/10.3390/ma13245737

[17] Mohammadi, M., Ashtiani, H. R. (2021). Influence of heat treatment on the Aa6061 and Aa6063 aluminum alloys behavior at elevated deformation temperature. Iranian Journal of Materials Science and Engineering, 18(2): 14-30. https://doi.org/10.22068/ijmse.1890

[18] Kumar, H., Prasad, R., Kumar, P., Tewari, S.P., Singh, J.K. (2020). Mechanical and tribological characterization of industrial wastes reinforced aluminum alloy composites fabricated via friction stir processing. Journal of Alloys and Compounds, 831: 154832. https://doi.org/10.1016/J.JALLCOM.2020.154832

[19] Tey, C.F., Tan, X., Sing, S.L., Yeong, W.Y. (2020). Additive manufacturing of multiple materials by selective laser melting: Ti-alloy to stainless steel via a cu-alloy interlayer. Additive Manufacturing, 31: 100970. https://doi.org/10.1016/J.ADDMA.2019.100970

[20] Rajesh Kannan, A., Siva Shanmugam, N., Rajkumar, V., Vishnukumar, M. (2020). Insight into the microstructural features and corrosion properties of wire arc additive manufactured super duplex stainless steel (ER2594). Materials Letters, 270: 127680. https://doi.org/10.1016/J.MATLET.2020.127680

[21] Pramono, A., Dhoska, K., Moezzi, R., Milandia, A. (2021). Ti/Sic based metal matrix composites by using self-propagating high temperatures synthesis (SHS). Revue des Composites et des Materiaux Avances, 31(3): 125-129. https://doi.org/10.18280/rcma.310302

[22] Ratanaphan, S., Olmsted, D.L., Bulatov, V.V., Holm, E.A., Rollett, A.D., Rohrer, G.S. (2015). Grain boundary energies in body-centered cubic metals. Acta Materialia, 88: 346-354. https://doi.org/10.1016/j.actamat.2015.01.069

[23] Hu, J., Zhuang, Z., Liu, F., Liu, X., Liu, Z. (2019). Investigation of grain boundary and orientation effects in polycrystalline metals by a dislocation-based crystal plasticity model. Computational Materials Science, 159: 86-94. https://doi.org/10.1016/j.commatsci.2018.12.010

[24] Gottstein, G., Shvindlerman, L.S. (2009). Grain Boundary Migration in Metals: Thermodynamics, Kinetics, Applications, Second Edition. Grain Boundary Migration in Metals. https://doi.org/10.1201/9781420054361

[25] Han, J., Thomas, S.L., Srolovitz, D.J. (2018). Grain-boundary kinetics: A unified approach. Progress in Materials Science, 98: 386-476. https://doi.org/10.1016/j.pmatsci.2018.05.004

[26] Faccoli, M., Roberti, R. (2013). Study of hot deformation behaviour of 2205 duplex stainless steel through hot tension tests. Journal of Materials Science, 48(15): 5196-5203. https://doi.org/10.1007/S10853-013-7307-8

[27] Pan, H., He, Y., Zhang, X. (2021). Interactions between dislocations and boundaries during deformation. Materials, 14(4): 1-48. https://doi.org/10.3390/ma14041012

[28] Patra, S., Ghosh, A., Kumar, V., Chakrabarti, D., Singhal, L.K. (2016). Deformation induced austenite formation in as-cast 2101 duplex stainless steel and its effect on hot-ductility. Materials Science and Engineering A, 660: 61-70. https://doi.org/10.1016/j.msea.2016.02.067

[29] Zhao, M., Huang, L., Li, C., Li, J., Li, P. (2021). Evaluation of the deformation behaviors and hot workability of a high-strength low-alloy steel. Materials Science and Engineering A, 810: 141031. https://doi.org/10.1016/j.msea.2021.141031

[30] Tran, T.T.T., Kannoorpatti, K., Padovan, A., Thennadil, S., Nguyen, K. (2021). Microbial corrosion of DSS 2205 in an acidic chloride environment under continuous flow. PLoS ONE, 16(5): e0251524. https://doi.org/10.1371/journal.pone.0251524

[31] Falodun, O.E., Mtsweni, E.B., Oke, S.R., Olubambi, P.A.

(2021). Influence of solution heat treatment on microstructure and mechanical properties of a hot-rolled 2205 duplex stainless steel. Journal of Materials Engineering and Performance, 30(10): 7185-7194. https://doi.org/10.1007/s11665-021-05904-z

[32] Haghdadi, N., Laleh, M., Kosari, A., Moayed, M.H., Cizek, P., Hodgson, P.D., Beladi, H. (2019). The effect of phase transformation route on the intergranular corrosion susceptibility of 2205 duplex stainless steel. Materials Letters, 238: 26-30. https://doi.org/10.1016/j.matlet.2018.11.143

[33] Shen, W., Wang, F., Yang, Z., Li, C., Lin, P., Zhu, X. (2020). Investigation of the Crack Initiation and Propagation in Super Duplex Stainless Steel During Hot Working. Minerals, Metals and Materials Series, 157-167. https://doi.org/10.1007/978-3-030-36540-0_15

[34] Zhang, Z., Jing, H., Xu, L., Han, Y., Gao, Z., Zhao, L., Zhang, J. (2017). Microstructural characterization and electron backscatter diffraction analysis across the welded interface of duplex stainless steel. Applied Surface Science, 413: 327-343. https://doi.org/10.1016/j.apsusc.2017.03.301

[35] Örnek, C., Engelberg, D.L. (2016). Correlative EBSD and SKPFM characterisation of microstructure development to assist determination of corrosion propensity in grade 2205 duplex stainless steel. Journal of Materials Science, 51(4): 1931-1948. https://doi.org/10.1007/s10853-015-9501-3

[36] Haghdadi, N., Cizek, P., Hodgson, P.D., Tari, V., Rohrer, G.S., Beladi, H. (2018). Effect of ferrite-to-austenite phase transformation path on the interface crystallographic character distributions in a duplex stainless steel. Acta Materialia, 145: 196-209. https://doi.org/10.1016/j.actamat.2017.11.057

[37] Mampuya, M.B., Umba, M.C., Mutombo, K., Olubambi, P.A. (2021). Effect of heat treatment on the microstructure of duplex stainless steel 2205. Materials Today: Proceedings, 38: 1107-1112. https://doi.org/10.1016/j.matpr.2020.06.196

[38] Haghdadi, N., Cizek, P., Hodgson, P.D., Beladi, H. (2019). Microstructure dependence of impact toughness in duplex stainless steels. Materials Science and Engineering A, 745: 369-378. https://doi.org/10.1016/j.msea.2018.12.117

[39] Claeys, L., De Graeve, I., Depover, T., Verbeken, K. (2020). Hydrogen-assisted cracking in 2205 duplex stainless steel: Initiation, propagation and interaction with deformation-induced martensite. Materials Science and Engineering A, 797: 140079. https://doi.org/10.1016/j.msea.2020.140079

[40] Haghdadi, N., Cizek, P., Beladi, H., Hodgson, P.D. (2017). A novel high-strain-rate ferrite dynamic softening mechanism facilitated by the interphase in the austenite/ferrite microstructure. Acta Materialia, 126: 44-57. https://doi.org/10.1016/j.actamat.2016.12.045

[41] Faccoli, M., Roberti, R. (2013). Study of hot deformation behaviour of 2205 duplex stainless steel through hot tension tests. Journal of Materials Science, 48(15): 5196-5203. https://doi.org/10.1007/s10853-013-7307-8

[42] Ou, X., Sietsma, J., Santofimia, M.J. (2020). Coalescence of martensite under uniaxial tension of iron crystallites by atomistic simulations. Materials Science and Technology (United Kingdom), 36(11): 1191-1199. https://doi.org/10.1080/02670836.2020.1762301

[43] Lin, Y.C., Huang, J., He, D.G., Zhang, X.Y., Wu, Q., Wang, L.H., Chen, C., Zhou, K.C. (2019). Phase transformation and dynamic recrystallization behaviors in a Ti55511 titanium alloy during hot compression. Journal of Alloys and Compounds, 795: 471-482. https://doi.org/10.1016/j.jallcom.2019.04.319

[44] Mazahery, A. (2018). Ways of describing grain boundaries and types of grain boundaries. Research Gate Technical Report.

[45] Breda, M., Brunelli, K., Grazzi, F., Scherillo, A., Calliari, I. (2015). Effects of cold rolling and strain-induced martensite formation in a SAF 2205 duplex stainless steel. Metallurgical and Materials Transactions A: Physical Metallurgy and Materials Science, 46(2): 577-586. https://doi.org/10.1007/s11661-014-2646-x

[46] Sohrabi, M.J., Naghizadeh, M., Mirzadeh, H. (2020). Deformation-induced martensite in austenitic stainless steels: A review. Archives of Civil and Mechanical Engineering, 20(4): 124. https://doi.org/10.1007/s43452-020-00130-1

[47] Yeddu, H.K. (2018). Phase-field modeling of austenite grain size effect on martensitic transformation in stainless steels. Computational Materials Science, 154: 75-83. https://doi.org/10.1016/j.commatsci.2018.07.040

[48] Singh, R. (2016). Applied Welding Engineering, Second Edition. Processes, Codes, and Standards, Elsevier Inc.

NOMENCLATURE

A/A	Austenite/Austenite
A/F	Austenite/Ferrite
bcc	Body-centred cubic
Cr	Chromium
DSS	Duplex stainless steel
EDS	Energy-dispersive spectrometry
F/F	Ferrite/Ferrite
fcc	Face-centred cubic
Fe	Iron
HABG	High-angle grain boundaries
K-S	Kurdjumov-Sachs
LAGB	Low angle grain boundaries
Mn	Manganese
Mo	Molybdenum
N-W	Nishiyama-Wassermann
SAGB	Special angle grain boundaries
SEM	Scanning electron microscope

Greek symbols

α	Alpha, Ferrite
α^{l}	Martensite
β	Beta
Υ	Gamma, Austenite